4-30-2020

Quantitative Resistance Assessment of SFRP-Strengthened RC Bridge Columns Subjected to Blast Loads

Ahmad Alsendi
Wayne State University, ahmad.alsendi@wayne.edu

Christopher D. Eamon
Wayne State University, eamon@eng.wayne.edu

Recommended Citation

Alsendi, A. and Eamon, C. D. 2020. "Quantitative resistance assessment of SFRP-strengthened RC bridge columns subjected to blast loads." *J. Perform. Constr. Facil.* 34 (4): 04020055. https://doi.org/10.1061/(ASCE)CF.1943-5509.0001458.

Quantitative Resistance Assessment of SFRP-Strengthened RC Bridge Columns Subjected to Blast Loads

Ahmad Alsendi[1] and Christopher D. Eamon[2]

Abstract

The blast resistance of a typical reinforced concrete bridge pier column design was modeled with a nonlinear finite element approach that considers material damage, fracture, and separation. While varying concrete strength, amount of longitudinal reinforcing steel, and gravity load, the effect of applying an externally bonded steel fiber reinforced polymer (SFRP) wrapping was assessed. The presented approach uniquely quantifies column blast resistance in terms of charge weight. It was found that blast capacity was roughly linearly related to concrete strength and steel reinforcement ratio, the former of which is most influential. It was further found that a single layer of SFRP modestly increased blast resistance, while additional SFRP layers provided minimal benefit.

Author Keywords:

concrete, columns, bridges, finite element analysis, blast, explosive load, FRP, SFRP.

----

1. Ph.D. candidate, Department of Civil & Environmental Engineering, Wayne State University, Detroit, MI, USA (corresponding author); ahmad.alsendi@wayne.edu
2. Associate Professor, Department of Civil & Environmental Engineering, Wayne State University, Detroit, MI, USA; eamon@eng.wayne.edu

Problem Introduction

To receive federal funding for construction and maintenance of vehicular and pedestrian bridge structures, State DOTs must meet the minimum design requirements provided in the American Association of State Highway and Transportation Officials *LRFD Bridge Design Specifications* (AASHTO LRFD 2017). As such, the vast majority of highway bridges in the United States are designed according to these standards. The limit states given in AASHTO to which bridge elements must be designed include various loads such as dead, live (vehicle and pedestrian), wind, seismic, as well as various others. Among these is blast loading (*BL*), which appears within the Extreme Event II limit state and is given a load factor of 1.0. This limit state also considers other possible impact loads from ice, vehicles, and ships on a bridge structure. Although blast load is identified and given a load factor, AASHTO provides no corresponding design criteria or recommendations for mitigation. Rather, AASHTO notes that blast load is a function of explosive charge characteristics as well as other parameters, and directs the designer to obtain any blast-related design requirements from the bridge owner.

Depending on the bridge geometry and size and placement of an explosive charge, any structural element may potentially experience damage, including superstructure components such as the deck and girders, as well as substructure elements such as abutments, piers, and the foundation. Of these, the central pier columns, an ubiquitous component of two span bridges crossing highways, are easily accessible and may cause complete collapse of both bridge spans if critically damaged. Because AASHTO does not specifically require consideration of blast load, the vast majority of bridge column designs within the US have not considered such loading. As most bridges likely face a very low threat to blast damage, this is perhaps appropriate. However, this accompanying lack of experience with blast loads as well as design provisions in AASHTO

LRFD require that engineers tasked with mitigating blast loads on bridge columns look to other sources for guidance.

Various researchers have recognized this need and studied this problem in the last two decades. The resulting research focused on several different bridge components including girders (Anwarul and Yazdani 2008; Cofer et al. 2010), decks (Lawver et al. 2003; Foglar and Kovar 2013; Foglar et al. 2017), a complete bridge (Winget el al. 2005), as well as columns (Williamson et al. 2011a, b; Williams et al. 2008; 2011; Williams 2009), where it was found that column geometry and reinforcement type, spacing, and splicing affected blast load resistance. Winget et al. (2005) and Yi et al. (2014) studied column failures and found that multiple modes are possible, including crushing or shearing of the column base; fracturing reinforcement; surface spalling; and plastic hinge formation. Much of the above research has been used to provide design guidance for bridge columns exposed to blast threats.

In this study, of particular concern is the large infrastructure of existing structures. If an existing bridge is found to experience an increased blast threat such that structural enhancement of the pier columns is warranted, it would be very costly to demolish and replace with a new, blast-resistant design. This would be especially undesirable if the superstructure is otherwise sound. In this case, a much cheaper, faster, and less disruptive retrofit option may be most feasible. To this end, several studies have explored retrofitting as a protective option. Malvar et al. (2007) examined the response of retrofitted columns with composite wraps or steel jackets under blast loading, and found that shear capacity could be enhanced. Later, Fujikura and Bruneau (2011) conducted blast tests on scaled reinforced concrete (RC) columns fit with steel jacketing, and determined that the columns did not exhibit ductile behavior under blast loading, but rather failed in base shear rather than flexural yielding. At about the same time, Heffernan et al. (2011)

subjected scaled RC columns to blast loads that were strengthened with composite wrapping formed of carbon or steel fibers. The authors found that not only carbon wrapping, but steel fiber reinforced polymer (SFRP) wrap could reduce the amount of concrete crushing that occurred in plastic hinge regions. More recently, Eamon and Alsendi (2017) conducted a cursory study on the blast resistance of SFRP columns, but few cases considered, with atypical wrapping application, unusual column boundary conditions, and coarse modeling, significantly limiting the usefulness of the results. SFRP has been previously studied for strengthening slabs for blast resistance as well, and was found to provide significant increase in resistance for these components (Silva and Lu 2007). Of these options, this study is focused on the SFRP alternative, which is not only ductile, but substantially less expensive than CFRP, and does not meaningfully increase column width as with most steel jacketing products. As summarized above, only a few numerical and experimental studies have investigated the effect of blast loads on SFRP-strengthened columns. Although this existing work is highly valuable, this topic remains significantly underexplored and the ability of SFRP to strengthen columns under blast, as well as the effect of typical design parameter changes on the blast resistance of unstrengthened columns, is greatly unquantified. As such, nearly all available results provide qualitative assessments or are relatively coarse (in a binary sense, either column failure or survival), leaving the specific change in column resistance to design parameter changes, such as SFRP strengthening, unknown.

Thus, the objective of this study is to estimate the blast resistance of typical bridge columns retrofitted with SFRP and compare the result to unmodified columns, in order to assess the potential benefit of this retrofit technique. In this process, a finite element analysis (FEA) approach is implemented to model hypothetical bridge columns subjected to blast. The effect of several design parameter changes on blast resistance are quantified, including the amount of longitudinal reinforcing steel, compressive strength of concrete, axial load on the column, as well as the use of SFRP strengthening.

Description of Bridge Columns Analyzed

Although column designs vary significantly, based on typical bridge structural geometries in the State of Michigan (Eamon et al. 2018), which are representative of many other states, columns in multi-column bridge piers are usually from 760 – 914 mm square with unsupported lengths from 3-5 m. The columns are linked together above by a pier cap (beam) which in turn supports the bridge girders, and the columns are supported below by a foundation. To represent the larger range of common highway bridge structures which are perhaps more prone to attack by blast, the upper range of these column dimensions were chosen for consideration in this study (914 mm square and 5 m unsupported length), providing a typical non-slender design (slenderness ratio L/r = 18.5, where L = unsupported length of column and r = radius of gyration), as shown in Figure 1.

The columns are assumed to have concrete compressive strength of $f'c$ = 42 MPa, with longitudinal reinforcement provided by 7 #8 (25 mm) bars per face for 24 bars total, which results in a reinforcing ratio (ρ) of 0.015. Stirrup ties (#4; 13 mm) are placed at 300 mm on center, with 50 mm cover. All steel is assumed to be Grade 60, with yield strength of 420 MPa. Additional design variations were also considered, with $f'c$ of 28 and 55 MPa, as well as longitudinal bar sizes of #11 (35 mm) and #14 (43 mm), with resulting reinforcement ratios of 0.029 and 0.042, respectively. Although these larger bar sizes are not commonly used, they were considered in this study to quantify the effect of changing reinforcing ratio.

The SFRP wrapping considered is based on commercially available products, where the composite is formed from unidirectional steel strands embedded in a thin polymer sheet to hold the fibers together. In the strong direction, the 1.2 mm thick composite sheets are taken to have a yield strength of 985 MPa and Young's modulus of 66.1 GPa, where in the weak direction, strength and stiffness are insignificant (Hardwire 2014). In practice, as with similar externally-bonded CFRP fabrics, after proper surface preparation, the column faces are coated with resin and then wrapped with SFRP. These systems are generally designed to increase the axial strength of an existing column by enhancing confinement strength. However, as noted above, such externally-bonded retrofit wraps have been repurposed to increase resistance to blast load as well, the focus of this study. Although more commonly used composite materials are available, the SFRP wrap is not only ductile but has about the same price as glass FRP, rendering it a less expensive alternative than more traditional CFRP wrapping. Two cases of wrapping are considered, where a single sheet and three sheets are applied. In both cases, the SFRP is applied to the column in the typical sense where the strong direction is oriented horizontally.

Models for Concrete and Reinforcement

Concrete constitutive relationships were modeled with the Johnson Holmquist Cook approach, a model developed for characterizing concrete behavior under large strains as well as high rates of strain and pressure (Holmquist 1993), conditions specifically associated with blast loading. In this model, pressure, strain rate, and accumulated damage affect concrete strength, where cumulative damage is a result of pressure and plastic strains experienced over time. The relationship between applied pressure and effective material stress is given by:

$$\sigma^{*} = [A(1-D) + BP^{*N}][1-Cln(\dot{\varepsilon}^{*})] \quad (1)$$

where σ^{*} is equivalent stress normalized to concrete compressive strength, given as $\sigma^{*} = \sigma / f'c$, where σ is normal stress; P^{*} is applied pressure, similarly normalized as $P^{*} = P / f'c$; D is cumulative damage, discussed further below; and $\dot{\varepsilon}^*$ is the normalized strain rate ($\dot{\varepsilon}^* = \dot{\varepsilon} / \dot{\varepsilon}_o$), such that $\dot{\varepsilon}$ is the actual rate of strain and $\dot{\varepsilon}_o$ a reference value of $1.0 s^{-1}$. Eq. 1 requires five material constants, which are the normalized cohesive strength (A); the normalized pressure hardening coefficient (B); the strain rate coefficient (C); the pressure hardening exponent (N); and the normalized maximum material strength (S_{MAX}). Damage (D) is a function of the cumulative equivalent plastic strain and volumetric strain, given as:

$$D = \sum [\Delta\varepsilon + \Delta\boldsymbol{\mu}_p / D_1 (P^* + T_H{}^*)^{D_2}] \qquad (2)$$

where $\Delta\varepsilon_p$ is equivalent plastic strain; $\Delta\boldsymbol{\mu}_p$ equivalent plastic volumetric strain; and $T_H{}^*$ the maximum tensile hydrostatic pressure, normalized to concrete strength as $T_H{}^* = T_H / f'c$. Three damage constants are used to calibrate the relationship to a specific material, and are given as D_1, D_2, and EF_{MIN}, where the latter constant specifies the plastic strain threshold needed for fracture damage initiation.

A final set of relationships are specified in the model to describe compressive hydrostatic pressure P as a function of volume change. Here, three regions are considered; initial linear elastic behavior, prior to concrete crushing ($P \leq P_{crush}$); linear inelastic behavior as pressure is increased, to represent the collapse of voids and pores within the concrete, but prior to complete collapse of all voids ($P_{crush} \leq P \leq P_{lock}$); and nonlinear inelastic behavior as P is further increased once all voids have been compressed ($P > P_{lock}$). The third region is described as:

$$P = K_1\bar{u} + K_2\bar{u}^2 + K_3\bar{u}^3 \qquad (3)$$

In the above limits, P_{crush} is the pressure corresponding to initial concrete crushing and loss of elastic behavior, given as: $P_{crush} = K * \mu_{crush}$, where K is the elastic bulk modulus and μ_{crush} the corresponding volumetric strain at crushing; and P_{lock} is the pressure at which all voids are collapsed. In Eq. 3, K_1-K_3 are material constants and $\bar{u}$ is a measure of volumetric strain, adjusted by the volumetric strain at P_{lock} (μ_{lock}): $\bar{u} = \bar{u} - \bar{u}_{lock} / 1 + \bar{u}_{lock}$. The material constants needed to define the model are taken from values obtained from concrete specimen test results given by Holmquist et al. (1993) and Williamson et al. (2011), and are summarized in Table 1.

A kinematic, elastic-plastic relationship is used to model reinforcing steel behavior. For all reinforcement, yield stress is specified as 450 MPa, Young's modulus as 200 GPa, and post-yield modulus as 20 GPa. Strain rate parameters are considered by using Cowper and Symonds model (Livermore 2018) which scales the yield stress with the factor:

$$1 + \left(\frac{\dot{\varepsilon}}{c}\right)^{1/p} \quad (4)$$

where $\dot{\varepsilon}$ is the strain rate, and strain rate parameters of 40.4 s^{-1} and 5.0 are taken for c and p, respectively (Bai and Jin 2016).

The SFRP sheet is modeled as anisotropic material with a yield stress of 985 MPa and elastic modulus of 66.1 GPa in the strong direction with Poisson ratio of 0.3, whereas the weak direction has insignificant strength and stiffness (corresponding properties taken as approximately 1/100th of the strong direction). Sheet thickness is taken as 1.20 mm (Hardwire 2014).

FEA Approach

The concrete material of the column was represented with a regular mesh of approximately 171,000 hexahedral elements (typical length 1.4 – 2.5 cm), whereas beam elements were used to model steel reinforcement. To avoid highly distorted elements and to simulate fracture debris, in addition to the concrete model above that includes strength and stiffness softening, once an element reaches a principal strain of 0.003, the element is taken to be so badly damaged that it is deleted from the model. Exposed element surfaces caused by deletion are bound by new contact surfaces, which prevent elements undergoing large displacements from penetrating others and allow fragmented pieces to collide. Similarly, contact surfaces are specified between beam elements representing reinforcing bars and solid concrete elements. Here, reinforcement is taken as completely bonded to the concrete until the surrounding concrete elements are disintegrated.

The SFRP material was modeled with shell elements, where it was assumed that the SFRP was applied to the lower half of the column only, where blast load is greatest for a charge placed on the ground (it was found that wrapping the entire column height made little difference in performance but significantly increased computational time). As with the beam elements for reinforcing modeling, the SFRP shells are linked to the model via contact surfaces to allow element interaction but prevent surface penetration. An SFRP shell element deletion criterion is specified as exceeding a longitudinal strain limit of 0.021, a value at which steel fiber rupture is expected to occur (Hardwire 2014).

The contact surface representing the SFRP bond initially rigidly links the SFRP shells to the concrete elements. When a specified failure criterion is reached, the slide surface releases the nodal constraints, allowing the shells to slide against or separate from the concrete surface. The failure criterion is given by:

$$\left(\frac{F_n}{F_{nf}}\right)^2 + \left(\frac{F_s}{F_{sf}}\right)^2 \geq 1 \qquad (5)$$

where F_n and F_s are the calculated normal (tensile) and shear stresses, respectively, while F_{nf} and F_{sf} are the normal and shear stress limits at failure. Here F_s is equal to the vector sum of the two shear components on the interface surface. The failure stress limits are based on typical resin properties, and are taken as F_{nf} = 32 MPa, and F_{sf} = 29.4 MPa. (**add Sika ref **). Once bond failure occurred, the coefficient of friction (μ) between the SFRP shells and concrete was varied from 0.3-0.7 in the model, but, as expected, no significant difference in ultimate blast capacity resistance was found as a function of μ.

The base of the column was taken as fully constrained to the ground, and the column top was constrained by attaching it to a simple beam element model of the surrounding pier cap and column frame system (as shown in Figure 1). These elements were given equivalent structural member properties based on the dimensions of the pier cap and column(s). To develop a representative dead load on the column, it is assumed that the pier supports a two-span, two-lane highway bridge where each span is 18.3 m long and the deck is 228 mm thick and 13 m wide, made of reinforced concrete, and supported by seven W36x170 steel girders. The pier is taken to be composed of 4 columns as shown in Figure 1, and the pier cap is 13 m long, 1 m high, and 0.9 m wide. These dimensions are similar to those of many highway bridges within Michigan as well as in other States. Based on this configuration, three different levels of axial load were applied to represent different gravity load scenarios: dead load only (DL), which includes the self-weight of the structure detailed above including barriers and diaphragms; the allowable nominal load on the structure (NL), taken as the total unfactored dead and live load that the column could support according to AASHTO LRFD criteria; and a maximum axial load (ML) that the column could resist according to its nominal capacity (Pn), given by:

$$Pn = 0.80\,[k_c f'c(A_g - A_{st})] + A_{st}f_y \qquad (8)$$

where k_c is the ratio of the maximum concrete compressive stress to the design compressive strength of concrete (0.85); $f'c$ is the compressive strength of concrete; A_{st} is the total area of longitudinal steel reinforcement; f_y is the yield stress; and A_g is the gross cross-sectional area. Although such a high load is not realistic from a design perspective, it was included to place a bound on possible column performance, which was found to be significantly influenced by axial load, as discussed in the results section. The dead load (DL) and allowable nominal load (NL) scenarios resulted in axial loads of 285 and from 14,000-30,000 kN, respectively, while the maximum load (ML) case varied as high as 24,500–52,000 kN, depending on the column design considered. Note the great discrepancy between the actual nominal gravity design loads (dead load = 285 kN; live load, based on the AASHTO HL-93 design vehicle load = 166 kN, for a total of 451 kN, and the allowable nominal load of 14,000-30,000 kN, indicative of how greatly overdesigned these bridge columns are for axial load); other design concerns such as vehicle collision, uniformity in construction for various bridges, and long-term maintenance typically dictate column section size.

No published data are available on typical charge standoff distances. Based on an inspection of approximately 100 blast-damaged structures in Iraq from 2014-2016 by the author, however, a significant variation in apparent charge placement was found. From these observations, the initiation point of the blast was taken as 50 mm above ground and approximately 1 m away from the column, a horizontal standoff distance which represented the average of those which could be identified.

The models were solved explicitly with a Lagrangian FEA formulation that allows for large strains and displacements as well as the separation, subsequent contact, and disintegration of elements using LS-DYNA (Livermore 2018).

Blast Load

The blast load model in this study is based on the CONWEP approach (Hyde 1988), which is formulated from a modified version of Friedlander's Equation fit to empirical data of blast pressures resulting from various charge weights and standoff distances (Kingery and Bulmash 1984). In this method, the resulting overpressure P, i.e. the air pressure over the ambient atmospheric pressure caused by the compressive shock wave from the blast, is modeled as a function of time (t) as:

$$P(t) = P_0 \left(1 - \frac{(t-t_a)}{t_d}\right) exp\ \left(-b\,\frac{(t-t_a)}{t_d}\right) \qquad (5)$$

where P_0 is peak overpressure; t_a the time of shock wave arrival; t_d the duration of the positive pressure phase, and b the decay coefficient, as shown in Figure 2. Time constants are a function of charge characteristics and placement, whereas b is determined by iteration during the analysis. When the shock wave strikes an object, rather than being absorbed, it may reflect and strike a second object. This second object may thus experience both side-on (direct) blast overpressure as well as reflected overpressure. The combination of these pressures may result in a significant increase over that generated by the direct blast. The total overpressure $P_T(t)$ resulting from the superposition of direct and reflected blast shock waves is given by:

$$P_T(t) = P_r(t)cos^2\theta + P_{so}(t)(1 + cos^2\theta - 2cos\theta) \qquad (6)$$

where, for $\cos\theta \geq 0$, $P_r(t)$ is the reflected blast overpressure; $P_{so}(t)$ the side-on overpressure as determined from Eq. 5 such that $P_{so}(t) = P(t)$; and θ the incidence angle between the blast wave and the normal of the reflecting surface. Although only a single structural element is exposed to blast in this study, Eq. 6 becomes relevant due to the presence of the ground, where as discussed above, the charge is located close to the ground and is thus modeled as a hemispherical surface burst that includes the reflected shock wave.

Approach Validation

Very few data are available that allow model validation. However, the general FEA approach described above was used in this study to successfully model column specimens exposed to blast load in previous research (Williamson et al. 2011). The experimental columns were similar to those considered in this study, although slightly smaller, with a 760 mm square cross section and height of 3.43 m. The columns were cast from 28.6 MPa concrete and reinforced with seven, 19 mm (#6) longitudinal bars per face and 13 mm (#4) stirrup ties spaced at 150 mm, with 25 mm cover. Bar yield strengths were 450 and 345 MPa for the longitudinal bars and ties, respectively. The cross-section is identical to that shown in Figure 1, except the side width is 0.76 m. The columns had a fixed base, a pinned top with no axial load, and were subjected to various blast loads initiated at the column base. A typical result is shown in Figure 3, where a test result is compared to the FEA model. The model result appears to be a reasonable representation of the general deformed shape, concentration of cracks, and locations of spalled concrete on the column. The model also appears to reasonably match the angle of the deformed reinforcement at the base of the column as well, most clearly seen from the exposed bar on the far right side. Only one quantitative value was reported for the experimental results, the maximum displacement of the column base at the end of the blast (approximately 5-6 ms). For the column shown, this was reported as 6.6 cm, while the analysis result was 7.1 cm. Given that a significant variation in strength exists even with static tests of nominally identical reinforced concrete specimens, analysis results were considered to be reasonably representative of column behavior and sufficiently accurate for assessment of performance for use in this study. Typical model solution time was approximately 18 minutes using ten 2.6GHz Intel processors in parallel and 5 GB of memory.

Failure Behavior

Using the modeling approach described above, the bridge pier column designs considered earlier were analyzed for blast resistance capacity, which is defined here as the maximum charge weight that the column could be subjected to and still support the axial load imposed. This was done by running multiple analyses, incrementing the charge weight up or down as required, to just cause a failure (i.e. collapse) condition. This critical charge weight (within a 1% tolerance) is then recorded. This specifically quantitative approach, to the knowledge of the authors, has not been previously considered in the evaluation of column blast capacity.

A typical result is shown in Figure 4 for a column with $f'c$= 41.4 MPa, ρ = 0.029, and axial load of 285 kN, at several points in time beyond blast initiation (at t=0), where the blast initiated at the bottom left of the column in the figures. Note in the figures, the supporting pier cap beam and adjacent columns (modeled as beam elements, as discussed above) are not shown for clarity. As shown, column failure is caused by base shearing and crushing. This column was exposed to the minimum charge weight just required to cause its collapse under the axial load. Although the exact shape and magnitude of the blast pressure profile vary across the face of the column, Figure 5 provides representative pressure curves at the column midheight, for a blast load just enough to fail the column ("minimum blast"), as well as a significantly larger blast load ("high blast") corresponding to a charge weight 3.5 times greater than that needed to fail the column. As shown in the figure, the blast pressure peaks at approximately 0.08 s, then decays to a (typically) briefly negative pressure at about 0.0875 s before rebounding, following the generally expected profile as shown in Figure 2.

At about the same time the peak pressure is reached, the concrete material at the column base is destroyed after extensive softening, and the column base is pushed away from the blast, bending the bottom longitudinal reinforcing bars. As the column base becomes eccentric relative to the top, the column slightly rotates counterclockwise, in turn causing some elements at the top right of the column to become crushed against the load plate representing the base of the pier cap. This phenomenon of member rotation causing crushing of the top material into a supporting component was similarly observed in concrete masonry walls subjected to blast (Eamon et al.

2004). This behavior is more evident in Figure 6, where the column is subjected to the higher level of load as shown in Figure 5, to be discussed further below. Mirroring the experimental deformation given in Figure 3, the column failure is thus caused by severe damage to the column base, characterized by base shifting, localized concrete cracking and crushing, and rebar bending, at which time the vertical load can no longer be supported.

A time-history of the column displacement is given in Figure 7 (“Base column, min blast” results), where a fairly nonlinear rate of vertical displacement is shown. Displacement (measured at the top of the column) begins to occur at approximately 0.06 s, slightly before the blast peak of 0.08 s, then the rate of collapse quickly increases soon afterwards. It is approximately at the blast peak that collapse initiates, when the bottom elements are destroyed and the reinforcement begins to bend, while at 0.12 s the reinforcement bends more significantly and the rate of collapse further increases. A similar response is seen for horizontal displacement (measured near the middle of the column) in Figure 8, although the rate of horizontal motion begins more rapidly as compared to the vertical motion.

Plastic strains in reinforcing bars near the bottom of the column are given in Figure 9. In the figure, labels are give the format: “Bar – Face, load level”, where “L” refers to a longitudinal bar and “T” a transverse bar; “F” a bar on the column side facing the blast and “B” on the back side of the column; and “high” and “min” to the two blast load levels considered as discussed earlier, and “SFRP” to columns so reinforced. For all cases, both longitudinal and transverse bars begin to yield at about same time of 0.07 s. Here plastic strains increase sharply then remain fairly constant (to a maximum level of about 0.0024) after the most severe deformation ends. For transverse bars, plastic strains are significant but not as quite as severe (to about 0.002). Strains in corresponding reinforcing bars on the face of the column opposite to the blast show a similar pattern, but the total deformation is much less, to about a half to a third in most cases.

To investigate the effect of a higher level of load on the failure behavior of the column, the significantly greater charge weight noted above (3.5 times the minimum necessary for failure) was applied as well. This result is given by Figure 6 and is also quantified in Figures 7-9 for comparison. As shown in the figures, the overall behavior is similar to that displayed at the lower load level, but with exaggerated effects, where failure occurs by concrete damage, sliding, and reinforcement bending at the base. Similarly, greater damage also occurs at the top of the column as it is rotated into the load plate. Additionally, a large diagonal “crack” near the base can be observed, as well as additional significant damage along the height of the column face adjacent to the blast. Here realize that many of the concrete elements experience damage and softening during the blast per the constitutive relationship given by the material model as discussed above; missing elements shown in the figures only represent those that have been so greatly deformed that they have lost all effective ability to transfer load and were thus removed from the model.

As shown in Figures 7 and 8, the displacement response of the column under high blast load is similar to that subjected to the minimum level. Here, as expected, the rate of displacement is greater, which is clear from a comparison of the deformation images given in Figures 4 and 6, although interestingly, differences in vertical displacement are more pronounced than horizontal. Close to the peak blast time, at approximately 0.075 s, as the base of the column is pushed inward, longitudinal bars facing the blast yield and quickly deform to a large maximum plastic strain of approximately 0.0027 (Figure 9). This large deformation can be seen in Figure 6. Transverse bars similarly begin to yield, though peak plastic strain are somewhat less. Similar to the low load level case, reinforcement strains on the opposite face are less than half of those facing the blast.

As expected, wrapping with SFRP requires a greater charge weight to fail the column. For example, the base column discussed above required approximately 86 kg of equivalent charge weight to fail, while the corresponding column wrapped with 1 layer of SFRP required 98 kg to just fail. The behavior of this column in shown in Figure 10, where at about the peak blast time, the SFRP strands that face the blast rupture (and thus these elements contribute insignificant stiffness and are removed from model), producing a few major horizontal "cracks" across the column face. The column then soon begins to collapse, but without the extensive base damage and horizontal shift seen with the unwrapped column. However, the blast does cause some slight rotation, causing the column top of column to crush against load plate. As shown in Figures 7 and 8, the displacement of the column is only slightly delayed with SFRP.

As shown in Figure 9, the SFRP wrapping significantly reduced strain in the reinforcement, from about a maximum plastic strain in the longitudinal bars from about 0.0025 (unwrapped) to about 0.0015, even though a higher blast load was required to fail the column. For transverse bars, maximum strains were reduced much further, to only a fraction of the non-wrapped case (from about 0.002 to 0.00025). This is not surprising, since the SFRP wrap is oriented horizontally and effectively acts as transverse reinforcement. As with the unwrapped column, strains are much lower on the opposite face of the blast. At the higher load level, a similar overall response occurs, but a larger portion of the concrete shell behind the SFRP wrap is crushed, with more extensive base damage, as shown in Figure 11.

It should be mentioned that, although not permitted by the AASHTO LRFD Specifications, removing the stirrup ties from the column design resulted in a very large drop in blast resistance. For example, for a model column with 42 MPa concrete strength and longitudinal reinforcement ratio of 0.029, blast capacity was reduced by approximately two thirds (from 97 kg to 30 kg of equivalent charge mass). Here it is apparent it the use of SFRP alone would not be an affective alternative to replacing stirrups.

Results of Parametric Analysis

Before the SFRP-wrapped columns were evaluated, a series of unwrapped columns were analyzed for blast failure load (in terms of equivalent charge weight) while varying several different design variables within the initial geometry considered. As discussed above, these were concrete strength (*f'c*), longitudinal steel reinforcement ratio (ρ), and axial load (P), for a total of 27 models (all combinations of three variations of each parameter). Figure 12 provides blast load resistance as a function of concrete strength, while Figure 13 graphs resistance in terms of reinforcement ratio. As shown in Figure 12, a fairly linear relationship between concrete strength and blast load resistance can be seen across a variety of reinforcement ratios and axial loads. It is interesting to note that the slope of the *f'c* vs resistance line is similar regardless of axial load or reinforcement ratio, indicating that change in *f'c* provides about the same absolute amount of capacity increase to blast, regardless of these other parameters. The result of this is, doubling concrete strength increases blast resistance by approximately 30-50%, where greatest proportional increases are seen for the least-reinforced columns loaded under dead load (DL) only, and least proportional increases are observed for columns most highly reinforced and under very high axial load (ML). Observing the results in Figure 13, it appears that the relationship between blast load resistance and steel reinforcement ratio is approximately linear. Following the same general relationship as with concrete strength, about the same absolute value of capacity increase to blast is seen as the amount of reinforcement is increased, regardless of concrete strength or axial load level. Blast capacity is less sensitive to reinforcement than concrete strength, however, as a 3.5

fold increase in reinforcing ratio provides a blast capacity increase of about 20 kg (with an initial charge weight resistance of approximately 65 to 105, depending on column configuration). Notice in both figures that as the applied axial load is increased, blast resistance is increased, albeit at a relatively slow rate. For a short column not governed by instabilities this is somewhat expected, where a high axial force effectively acts as a restraint, 'clamping' the column down and inhibiting the horizontal displacement which ultimately leads to collapse. Here is should be noted that shorter (3 m tall) columns with otherwise identical design parameters were also studied, and only very small increases in blast resistance were found over the 5 m tall columns. It was determined that this occurred because both the 3 m and 5 m columns are significantly within the 'short' column range, where capacity is governed by material strength rather than instability.

Results for the SFRP-wrapped columns subjected to axial dead load (DL), the expected gravity load condition, are given in Figure 14, where 18 model results are summarized (three variations each of $f'c$ and ρ, and two SFRP layer arrangements). Applying one layer of SFRP provided a modest increase in blast capacity from approximately 10%-15% depending on the column variation considered; columns with initially higher capacities experienced a somewhat greater benefit in terms of additional charge weight that could be resisted with the same amount of SFRP. The increase in capacity provided is about equivalent to doubling the amount of longitudinal steel. As shown in the figure, three layers of SFRP were also applied in the model, which resulted in blast capacity increases from only about 1% to 3%. Larger increases in blast capacity from SFRP were observed under higher axial load conditions, up to 30% in some cases, but such high axial load cases are not reasonably expected in practice.

Conclusions

The blast resistance of a typical larger bridge pier column was modeled, and the impact of changes in concrete strength, amount of longitudinal reinforcing steel, gravity load, and application of SFRP wrapping were quantified. Blast capacity was found to be a roughly linear function of concrete compressive strength, where doubling concrete strength increases blast capacity from about 30-50%. Similarly, reinforcement content is approximately linearly related to blast resistance but results are less sensitive, where increasing reinforcement ratio by a factor of approximately 3.5 results in a resistance increase of 10-20%. Increasing axial load on the short columns studied was also found to increase blast resistance. A single layer of SFRP, applied on the lower half of the column closest to the blast loads considered, increased capacity by a range from 10%-15% with typical axial loads applied. Additional SFRP layers provided an insignificant increase in resistance. Thus, for new construction, of the parameters investigated, increasing concrete strength appears to be most effective. For retrofits, although SFRP is relatively inexpensive compared to common alternatives, it appears to provide modest gains on the column geometry studied.

Data Availability

All data, models, and code generated or used during the study appear in the submitted article.

References

AASHTO. (2017). *LRFD Bridge Design Specifications*, 8th Ed., Washington, D.C.

Alhadid, M., Soliman, A., Nehdi, M., and Youssef, M. (2014). "Critical Overview of Blast Resistance of Different Concrete Types." *Institution of Civil Engineers, Magazine of Concrete Research,* 66(2):72-81.

ATBlast Software (2003). *Applied Research Associates (ARA), Inc*.

Bai, Y., and Jin, W. (2016). Marine Structural Design, *second edition*.

Cofer, W., Matthews, D., and McLean, D. (2010). "Effects of blast loading on prestressed girder bridges." *Shock and Vibration*, 19(1):1-18.

Eamon, C., and Alsendi, A. (2017). "Resistance of Columns Subjected to Blast Loads." *Builder*, PWB Media Zdzieblowski, December, pp. 78-81.

Eamon, C., Baylot, J., and O'Daniel, J. (2004). "Modeling Concrete Masonry Walls Subjected to Explosive Loads." *ASCE Journal of Engineering Mechanics*, 10.1061/(ASCE)0733-9399(2004)130:9(1098).

Eamon, C., Darwish, I., and Alsendi, A. (2018). "Development of Secondary Route Bridge Design Plan Guides." Michigan Department of Transportation Report SPR-1669.

Foglar, M., Hajek, R., Fladr, J., Pachman, J., and Stoller, J. (2017). "Full-scale experimental testing of the blast resistance of HPFRC and UHPFRC bridge decks." *Construction and Building Materials*, 145:588-601.

Foglar, M., and Kovar, M. (2013). "Conclusions from experimental testing of blast resistance of FRC and RC bridge decks." *International Journal of Impact Engineering*, 59:18-28.

Fujikura, S., and Bruneau, M. (2011). “Experimental investigation of seismically resistant bridge piers under blast loading.” *ASCE Journal of Bridge Engineering*, 10.1061/ (ASCE)BE.1943-5592.0000124.

Fujikura, S., Bruneau, M., and Lopez-Garcia, D. (2008). “Experimental investigation of multihazard resistant bridge piers having concrete-filled steel tube under blast loading.” *ASCE Journal of Bridge Engineering*, 10.1061/(ASCE)1084-0702(2008)13:6(586).

Ha, J., Yi, N., Choi, J., and Kim, J. (2011). “Experimental Study on Hybrid CFRP-PU Strengthening Effect on RC Panels Under Blast Loading.” *Composite Structures* 93: 2070-2082.

Hardwire Armor Systems: Hardwire tapes. Pocomoke City MD. https://www.hardwirellc.com, accessed 2014.

Heffernan, P., Wight, G., and Erki, M.-A. (2011). “Research on the Use of FRP for critical load-bearing infrastructure in conflict zones.” *ASCE Journal of Composites for Construction*, 10.1061/(ASCE)CC.1943-5614.0000077.

Holmquist, T., Johnson, G., and Cook, W. (1993). “A computational constitutive model for concrete subjected to large strains, high strain rates, and high pressures.” *Proc., 14th International symposium, Warhead mechanisms, terminal ballistics; 1993; Quebec; Canada*, 2:591-600.

Hyde, D. (1988). *User's Guide for Microcomputer Program CONWEP, Applications of TM 5-855-1*, Fundamentals of Protective Design for Conventional Weapons. SL-88-1, U.S. Army Corps of Engineers Waterways Experiment Station Instruction, Vicksburg, MS.

Kingery, C., and Bulmash, G. (1984). *Air-Blast Parameters from TNT Spherical Air Burst and Hemispherical Surface Burst*. ARBRL-TR-02555, U.S. Army Ballistic Research Laboratory, Aberdeen Proving Ground, MD.

K.M. Anwarul Islam, A. and Yazdani, N. (2008). “Performance of AASHTO girder bridges under blast loading.” *Engineering Structures*, 30:1922-1937.

Malvar, L., Crawford, J., and Morrill, K. (2007). “Use of composites to resist blast.” *ASCE Journal of Composites for Construction*, 10.1061/(ASCE)1090-0268(2007)11:6(601).

Lawver, D., Daddazio, R., Oh, G. J., Lee, C.K.B., Pifko, A. B., and Stanley, M. (2003). “Simulating the response of composite reinforced floor slabs subjected to blast loading.” *Proc., 2003 ASME International Mechanical Engineering Congress, ASME, New York*, 10.1115/IMECE2003-43870.

Livermore Software Technology Corporation. (2018). *LS-DYNA keyword user’s manual, version 971*, Livermore, CA.

Marchand, K., Williamson, E., and Winget, D. (2004). “Analysis of blast loads on bridge substructures.” *Structures under shock and impact*, 8:151-160.

Mutalib, A., and Hao, H. (2011). “Numerical Analysis of FRP-Composite-Strengthened.” *ASCE, Journal of performance of constructed facilities*, 10.1061/(ASCE)CF.1943-5509.0000199.

Nasim Uddin (2010). *Blast Protection of Civil Infrastructures and Vehicles Using Composites*.

Orton, S., Chiarito, V., Minor, J., and Coleman, T., (2014). “Experimental Testing of CFRP-Strengthened.” *ASCE Journal of Structural Engineering*, 10.1061/(ASCE)ST.1943-541X.0000821.

Randers-Pehrson, G., and A. Bannister, K. (1997). *Airblast Loading Model for DYNA2D and DYNA3D*, Defense Technical Information Center, U.S. Army Ballistic Research Laboratory, Aberdeen Proving Ground, MD.

Rutner, M., Astaneh-asl, A., and Son, J. (2006). “Blast resistant performance of steel and composite bridge piers.” 10.2749/222137806796185346.

Silva, P., and Lu, B. (2007). “Improving the Blast Resistance Capacity of RC Slabs With Innovative Composite Materials.” *Composites* 38:523-534.

Son, J., and Astaneh-Asl, A. (2012). "Blast Resistance of Steel Orthotropic Bridge Decks." *ASCE Journal of Bridge Engineering*, 10.1061/(ASCE)BE.1943-5592.0000283.

Son, J., and Lee, H-J. (2011). “Performance of cable-stayed bridge pylons subjected to blast loading.” *Engineering Structures,* 33:1133-1148.

Winget, D., Marchand, K., and Williamson, E. (2005). “Analysis and design of critical bridges subjected to blast loads.” *ASCE Journal of Bridge Engineering*, 10.1061/(ASCE)0733-9445(2005)131:8(1243).

Williamson, E., Bayrak, O., Davis, C., and Williams, G. (2011). “Performance of bridge columns subjected to blast loads. I: experimental program.” *ASCE Journal of Bridge Engineering*, 10.1061/(ASCE)BE.1943-5592.0000220.

Williamson, E., Bayrak, O., Davis, C., and Williams, G. (2011). “Performance of bridge columns subjected to blast loads. II: results and recommendations.” *ASCE Journal of Bridge Engineering*, 10.1061/(ASCE)BE.1943-5592.0000221.

Williams, G., Holland, C., Williamson, E., Bayrak, O., Marchand, K., Ray, J. (2008). “Blast-resistant highway bridges: design and detailing guidelines.” *WITPress, Ashurst Lodge, Ashurst, Southampton, United Kingdom*, 98:75-83.

Williams, G. (2009). ”Analysis and response mechanisms of blast loaded reinforced concrete columns.” Ph.D. dissertation, Univ. of Texas at Austin.

Williams, G., and Williamson, E. (2011). “Response of reinforced concrete bridge columns subjected to blast loads.” *ASCE Journal of Bridge Engineering*, 10.1061/ (ASCE)ST.1943-541X.0000440.

Wu, C., Oehlers, D., Rebentrost, M., Leah, H., and Whittaker, A. (2009). “Blast testing of Ultra-High Performance Fiber Concrete Slabs and FRP Retrofitted RC Slabs.” *Engineering Structures*, 31:2060-2069.

Yi, Z., Agrawal, A., Ettouney, M., and Alampalli, S. (2014) “Blast load effects on highway bridges. I: modeling and blast load effects.” *ASCE Journal of Bridge Engineering*, 10.1061/(ASCE)BE.1943-5592.0000547.

Yi, Z., Agrawal, A., Ettouney, M., and Alampalli, S. (2014) “Blast load effects on highway bridges. II: failure modes and multihazard correlations.” *ASCE Journal of Bridge Engineering*, 10.1061/(ASCE)BE.1943-5592.0000548.

List of Tables

List of Figures

Table 1. Concrete Model Parameters.

Parameter	Value	Parameter	Value
A	0.79	T	2.3, 3.5, 4.6 MPa*
B	1.6	P_{crush}	9.2, 13.8, 18.4 MPa*
C	0.007	u_{crush}	3.9, 5.8, 7.7x10^{-6}*
N	0.61	P_{lock}	800 MPa
S_{MAX}	7.0	u_{lock}	0.1
D_1	0.04	K_1	85000 MPa
D_2	1.0	K_2	-171000 MPa
EF_{MIN}	0.01	K_3	208000 MPa

*For concrete strengths of 28, 41, and 55 MPa, respectively.

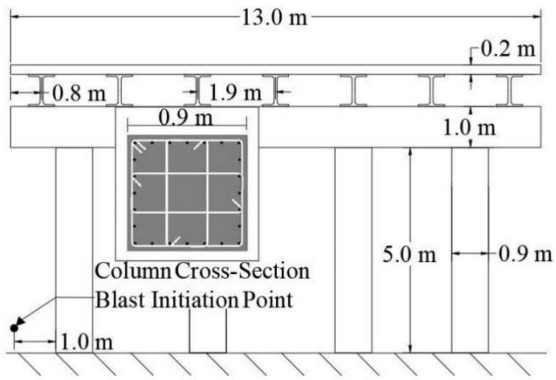

Figure 1. Elevation View of Bridge Pier.

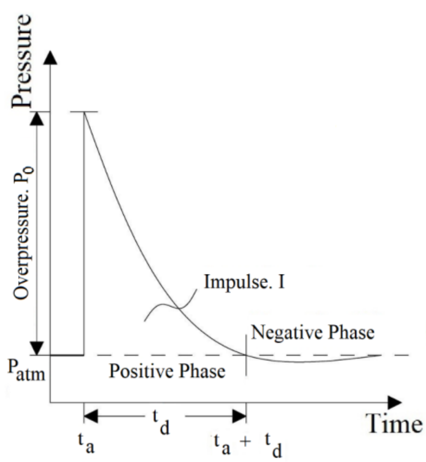

Figure 2. Typical Blast Wave Pressure Time History.

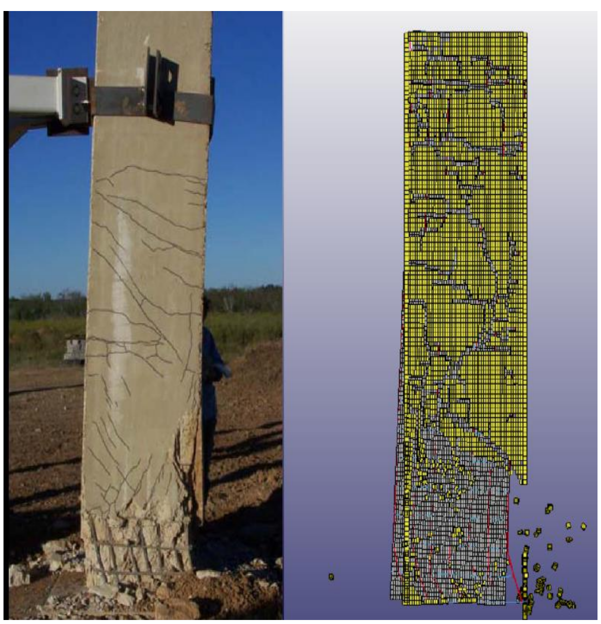

Figure 3. Experimental and FEA Results.

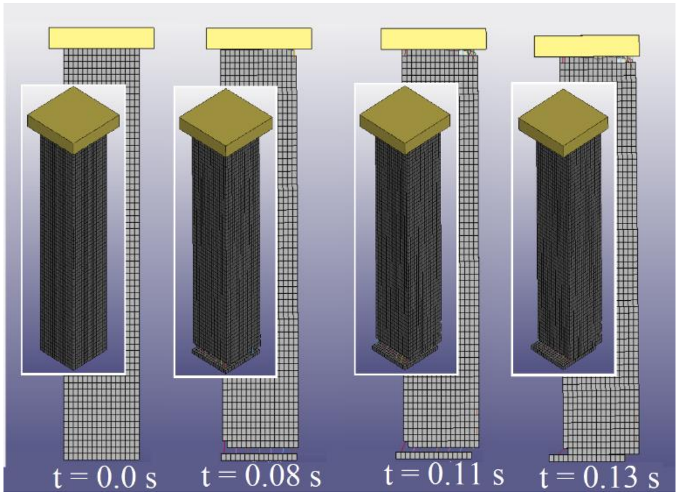

Figure 4. Typical Response of Column (Minimum Blast Load for Collapse).

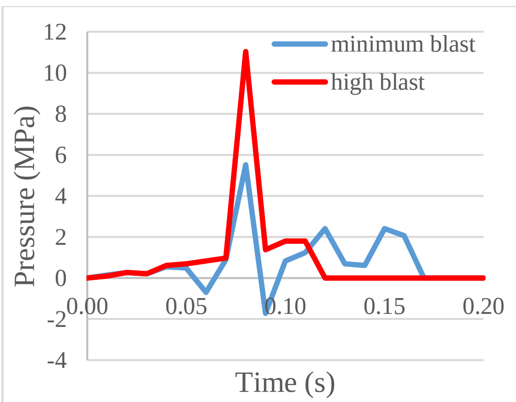

Figure 5. Typical Time-Pressure Relationships Experienced by Column.

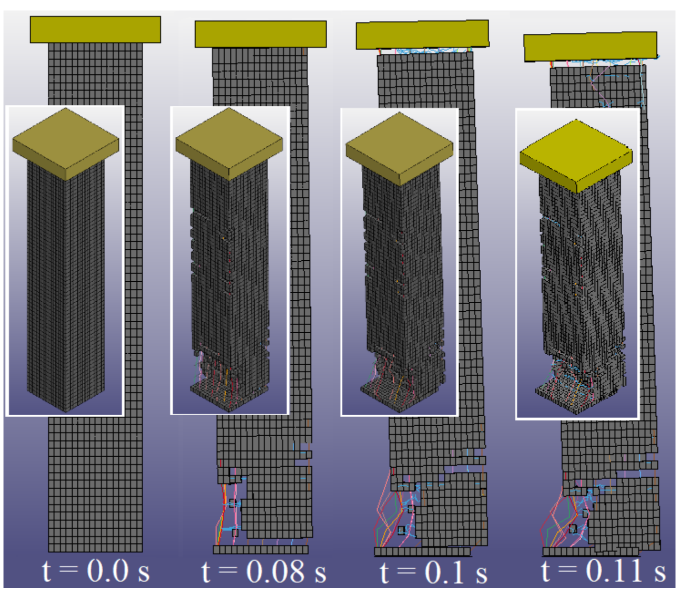

Figure 6. Typical Response of Column (High Blast Load).

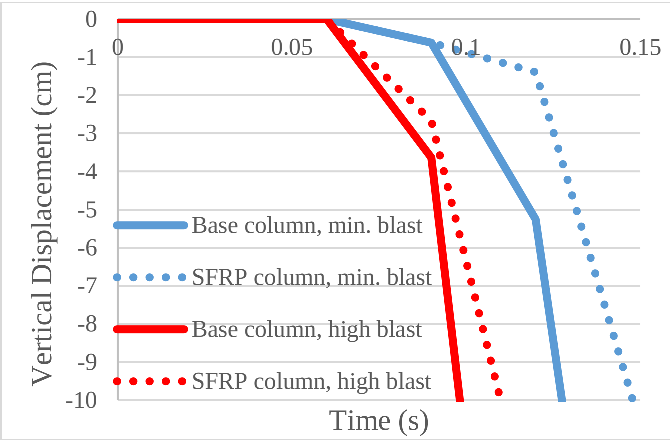

Figure 7. Vertical Displacement.

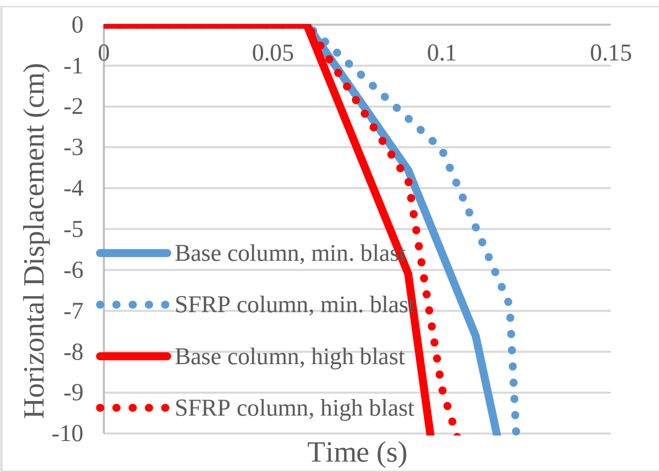

Figure 8. Horizontal Displacement.

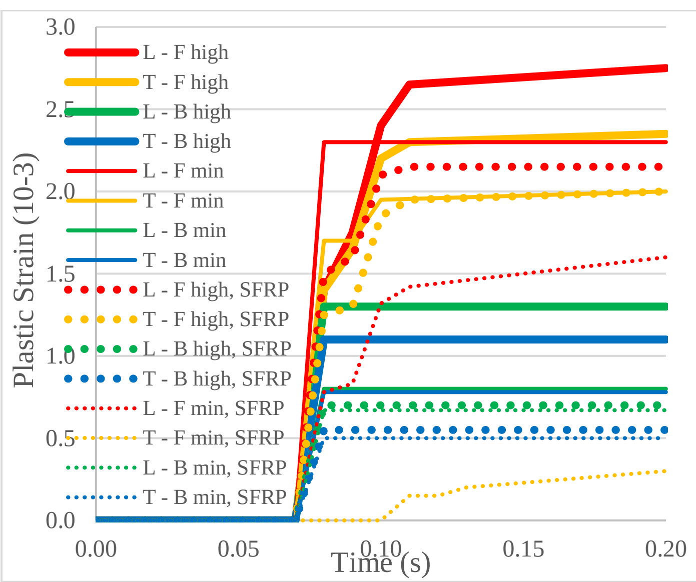

Figure 9. Reinforcing Bar Strains.

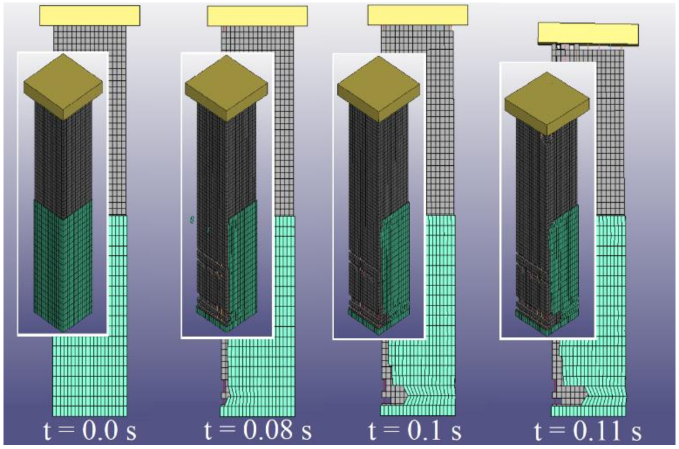

Figure 10. Typical Response of Column Wrapped with SFRP (Minimum Blast Load for Collapse).

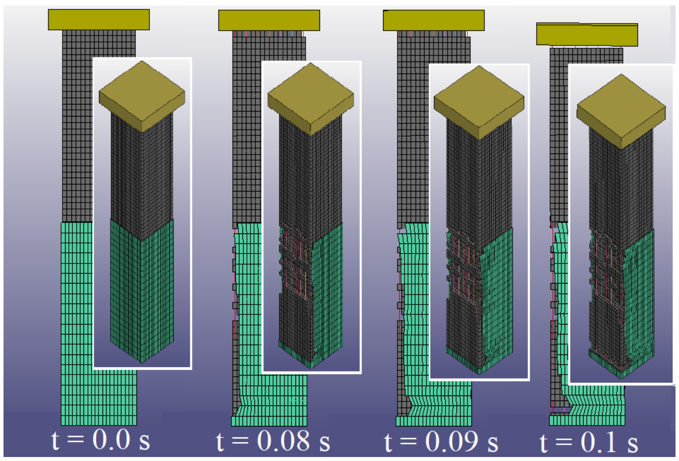

Figure 11. Typical Response of Column Wrapped with SFRP (High Blast Load).

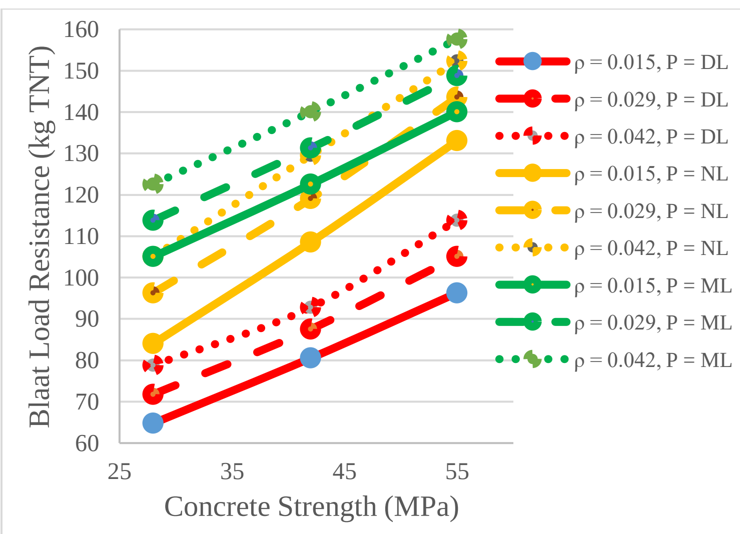

Figure 12. Column Blast load Resistance as a Function of Concrete Strength.

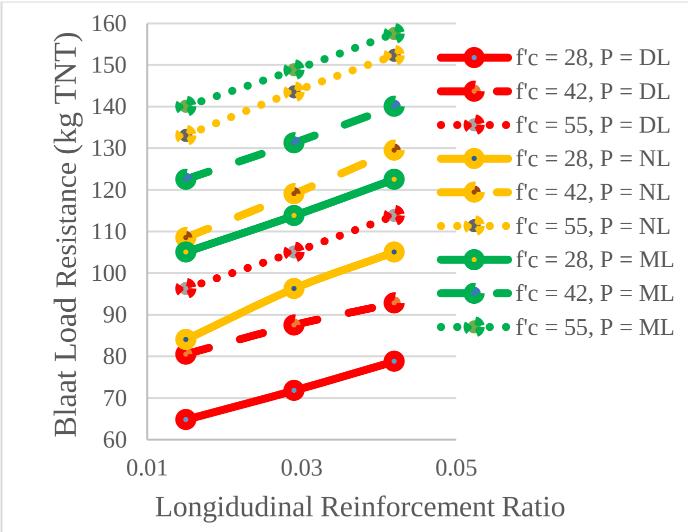

Figure 13. Column Blast load Resistance as a Function of Longitudinal Reinforcement Ratio.

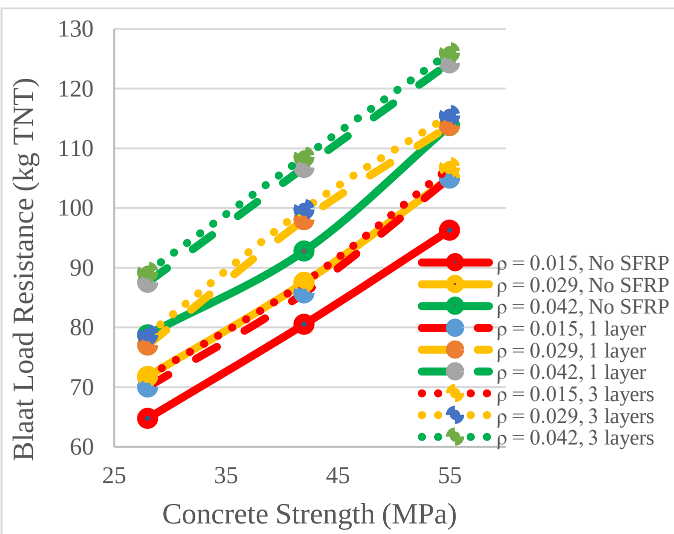

Figure 14. SFRP-Wrapped Column Blast Resistance.